Journal of Materials Chemistry A

Accepted Manuscript

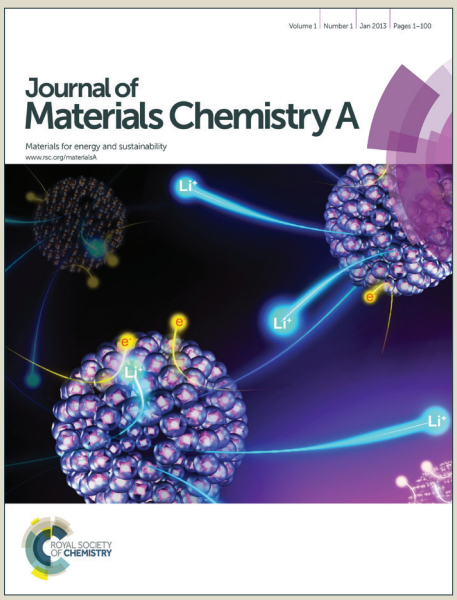

ROYAL SOCIETY OF CHEMISTRY

www.rsc.org/materialsA

Journal of Materials Chemistry A

Dynamic Article Links ►

Cite this: DOI: 10.1039/c0xx00000x

PAPER

www.rsc.org/xxxxxx

Highly Crystalline Fe_2GeS_4 Nanocrystals: Green Synthesis and Their Structural and Optical Characterization†

Bo-In Park,[‡a,b] Seunggun Yu,[‡a,c] Yoonjung Hwang,[d,e] So-Hye Cho,[a,e] Jae-Seung Lee,[b] Cheolmin Park,[c] Doh-Kwon Lee,*[d,e] and Seung Yong Lee,*[a,e]

Received (in XXX, XXX) Xth XXXXXXXXX 20XX, Accepted Xth XXXXXXXXX 20XX
DOI: 10.1039/b000000x

The olivine Fe_2GeS_4 compound has attracted much attention as a thermodynamically stable derivative of pyrite FeS_2, which has been studied extensively as an earth-abundant light-absorbing candidate material. Nevertheless, reports on nanocrystalline Fe_2GeS_4 and its optoelectronic properties are limited. Herein, Fe_2GeS_4 nanocrystals are synthesized via a solvent-free mechanochemical process. This process not only reduces the synthesis time, but it also avoids the use of hazardous solvents, thereby mitigating environmental concerns. The crystallinity of the synthesized nanocrystals is significantly enhanced by a post heat treatment in a sulfur-containing atmosphere, showing no phase decomposition. Lattice-resolved micrographs reveal that the post-annealed nanocrystals have a hexagonal-faceted platelet structure with (002) base planes. The oxide layer near the surface region is removed by the post-annealing process, most likely due to the replacement of oxygen with sulfur in the controlled atmosphere. The post-annealed Fe_2GeS_4 nanocrystals clearly exhibit an optical band gap of 1.43 eV and near-band-edge photoluminescence emission at 1.41 eV. This is the first experimental demonstration of the Fe_2GeS_4 nanocrystals having optoelectronic properties that are suitable for solar applications.

Introduction

The constant hunt for competitive photovoltaic materials has fueled research on innovative thin-film materials, such as CdTe, $Cu(In,Ga)S_2$, and Cu_2ZnSnS_4.[1–4] Recently, iron persulfide (FeS_2) in a pyrite structure has attracted significant interest owing to its advantages as a photovoltaic absorber layer, such as its elemental abundance, structural simplicity, straightforward synthetic route, high absorption coefficient (~ 10^5 cm^{-1}) and reasonably appropriate band gap (~ 0.95 eV).[5–8] Despite the potential of FeS_2 as an absorber layer, however, it remains but 'fool's gold' due to its unstable surface, which exhibits a sulfur deficiency.[9] The dangling bond of the sulfur atom forms FeS, which has a very small band gap and thus results in low photo-voltage in devices.[9–12] Recently, Yu et al. demonstrated the theoretical possibility of alternative iron chalcogenides, including Fe_2GeS_4 and Fe_2SiS_4, to replace the deficient pyrite structure for use in photovoltaics.[13] Fe_2GeS_4 crystallizes in the olivine structure, as shown in Fig. 1a (*P*nma with a = 1.24 nm, b = 0.72 nm, and c = 0.58 nm), where sulfur anions form a hexagonal close-packed structure and iron and germanium cations occupy half of the octahedral sites and an eighth of the tetragonal sites. In addition to retaining the attractive properties of pyrite, including a high absorption coefficient (> 10^5 cm^{-1}), the Fe_2GeS_4 compound is predicted to have a more suitable band gap (1.40 eV) to harvest solar energy[14] as well as better structural stability in comparison to pyrite.[13]

To magnify the advantages of Fe_2GeS_4 as a low-cost absorber, inexpensive fabrication methods would be required. In this regard, nanocrystal-based thin-film fabrication routes have attracted a great deal of attention due to their potential to realize low-cost, printable devices.[15] The nanocrystalline ink approach may offer additional advantages, such as a uniform, well-controlled film composition and fewer impurities due to the use of nanocrystals (NCs) with a well-defined stoichiometry and a high reactivity. Fredrick and Prieto recently reported for the first time Fe_2GeS_4 NCs synthesized via a wet-chemical method.[16] Their colloidal NCs demonstrated the possibility of generating a photocurrent with a modest potential. However, their solution-based synthesis approach leaves something to be desired in terms of throughput and the simplicity of the process. Alternatively, the dry mechanochemical process (ball milling) can provide a more rapid and simple route to synthesize Fe_2GeS_4 NCs compared to multistep solvent-based methods.[17,18] Moreover, the dry mechanochemical method is compatible with the current green-chemistry agenda, avoiding the use of expensive and hazardous organic solvents during the synthetic process.[19]

In this work, we present a green and facile synthesis of Fe_2GeS_4 NCs via a solvent-free mechanochemical process. Single-crystalline Fe_2GeS_4 NCs were synthesized with high crystallinity from elemental powder precursors. We also demonstrate that the crystallinity of the synthesized NCs is

greatly enhanced and that concerns about the surface oxidation of NCs can be alleviated by a post heat treatment. Interestingly, the post-annealing process induced a change in the morphology of NCs into hexagonal-faceted platelets. Opto-physical measurements showed a clear absorption edge of the NCs at around 1.43 eV.

Experimental Section

Preparation of Fe_2GeS_4 NCs via a mechanochemical method

To synthesize Fe_2GeS_4 NCs, elemental powders of iron (Alfa Aesar, 99.998%, 22 mesh), germanium (Alfa Aesar, 99.999%, 100 mesh), and sulfur (Sigma Aldrich, 99.998%, 100 mesh) were used as precursors. The elemental precursors were weighed under an argon atmosphere in a glove box to yield the following ratio: Fe : Ge : S = 2 : 1.5 : 4. Five grams of the metallic precursor mixture was added to an 80-mL stainless steel jar containing 50 g of zirconia balls (25 g of 5-mm diameter balls and 25 g of 10-mm diameter balls). The jar was then placed in a planetary ball-milling machine (Fritsch GmbH, Pulverisette 6). The mechanochemical processes for the synthesis of the Fe_2GeS_4 NCs were performed at 550 rpm. The obtained Fe_2GeS_4 NCs were post-annealed at 450 °C for 2 h in a tube furnace under a H_2S (1%) gas atmosphere.

Characterization

A Bruker D8 Advance XRD device (Cu K_α radiation, λ = 1.5406 Å) was used to obtain the X-ray diffraction (XRD) patterns of the obtained Fe_2GeS_4 NCs. The phase purity of the synthesized NCs was further examined by Raman spectroscopy using a Horiba Jobin-Yvon LabRam Aramis spectrometer equipped with an Ar laser source (λ = 514.5 nm). The morphologies of the Fe_2GeS_4 NCs were investigated using an FEI Inspect F50 FE-SEM device at acceleration voltages of 10 kV to 15 kV. High-magnification images, selected-area electron diffraction (SAED) patterns, and energy dispersion spectroscopy (EDS) data were obtained using a TEM (FEI Titan 80-300 microscope) operating at 300 kV. For the XPS analysis, pellets (10 mm in diameter, 1 mm in thickness) of the Fe_2GeS_4 NCs were prepared. An ULVAC-PHI PHI 5000 VersaProbe device was employed with a monochromated Al K_α X-ray source of 1486.6 eV with a C 1s peak of 286.6 eV used for calibration as the energy reference for the XPS analysis. The optical absorption properties of the obtained Fe_2GeS_4 NCs were characterized by a VARIAN Cary 5000 UV/Vis/NIR spectroscopy apparatus. The photoluminescence (PL) spectra of powder samples were measured with a Hitachi F-7000 spectrophotometer using 532 nm line of Xe lamp as an excitation source.

Results and Discussion

Fig. 1b shows the XRD patterns of powders milled for various periods of time. It is shown that for as much as 8 h of milling, only the elemental precursors were detected. Abrupt and significant changes of the constituent phases were first recognized in the powder milled for 10 h. Most of the peaks that appeared at 10 h were found to belong to the olivine Fe_2GeS_4 phase (denoted by ★, JCPDS card no. 04-007-5444). A trace amount of elemental Ge (denoted by ◆) remained unreacted at

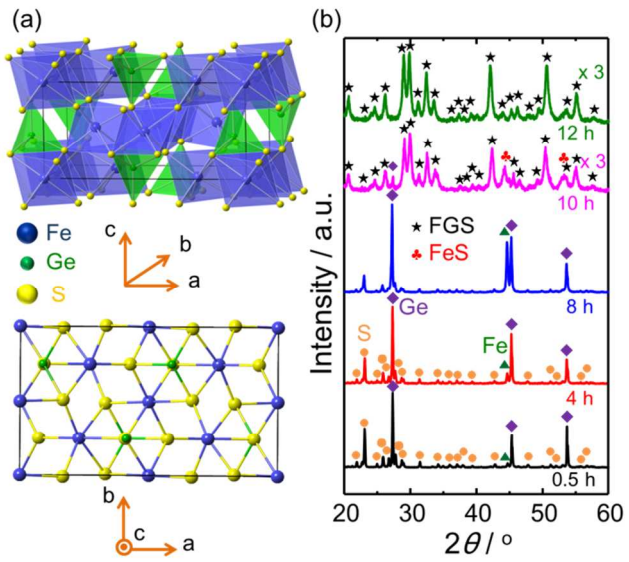

Fig. 1. (a) Crystal structure of Fe_2GeS_4 and (b) XRD patterns of the milled products as a function of the milling time.

10 h. In addition, the peaks at about 44 ° and 53 ° (♣) can be assigned to the binary FeS phase (JCPDS card no. 03-065-1894). The elemental Ge and the FeS secondary phases finally disappeared at 12 h, leaving only a single phase of Fe_2GeS_4 in the milled power. No further changes in the XRD pattern were identified upon further milling for more than 12 h. The microstructural evolution as a function of the milling time (Fig. S1 in the Electronic Supplementary Information, ESI) was consistent with the phase evolution observed with XRD patterns. The elemental precursors (*ca.* 50 μm in diameter) were gradually fragmented and pulverized with an increase in the milling time to 8 h. The powder milled for 8 h was found to consist of submicron particles as well as their agglomerates of a few micrometers. Further milling up to 10 h led to no appreciable changes in the morphology of the milled products, although it resulted in sudden phase changes, as shown in Fig. 1b. Thus, 2 h of additional milling of powder milled for 8 h is thought to provide pulverized particles with sufficient energy to induce the self-ignition and propagation of chemical reactions.[20,21]

According to these observations, the morphological change and the phase evolution during the mechanochemical synthesis of Fe_2GeS_4 NCs can be summarized as schematically illustrated in Fig. 2. The precursor materials are pulverized to the submicron level by the grinding media over the milling period, while mechanical stress is continuously applied to the surfaces of the particles. When the particle size decreases to a certain point, the mechanical energy is regarded to become sufficient so as to overcome the activation barrier and thus initiate chemical reactions. Once the spontaneous formation of a new product (Fe_2GeS_4) takes place, the exothermic heat associated with the formation enthalpy (–51.4 kJ mol^{-1})[13] allows the reaction to be completed in 2 h. The sudden appearance of Fe_2GeS_4 along with secondary phases and the gradual disappearance of the secondary phases are in agreement with the characteristic features observed during the mechanochemical process.[22,23] It is emphasized here

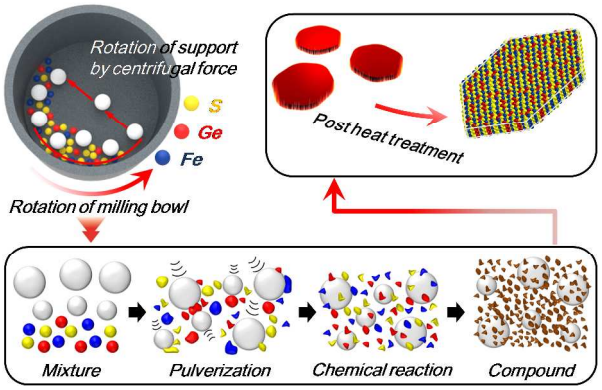

Fig. 2. Schematic illustration of the synthesis of Fe_2GeS_4 NCs by a mechanochemical process, including sequential pulverization and chemical reactions. The as-synthesized Fe_2GeS_4 NCs were post-annealed to have higher crystallinity.

that the present mechanochemical process for synthesizing Fe_2GeS_4 NCs is simple and environmentally friendly, as no organic solvents or additives are employed. In addition, the present method is rapid in comparison with previous reports in which a time of more than 24 h is required to synthesize the Fe_2GeS_4 phase.[13,16] Interestingly, compositional analysis by TEM for the olivine nanocrystals revealed that the ratio of Fe to Ge was 1.3, which is close to the ratio of the input precursors (Fig. S2 in the ESI). This analysis implies that Ge may have its broad solubility range from 1 to 1.5 in the Fe_2GeS_4 olivine structure.

In an attempt to enhance the crystallinity of the as-synthesized Fe_2GeS_4 NCs, a post-annealing process was carried out. The XRD pattern of the post-annealed Fe_2GeS_4 NCs is shown in Fig. 3a, where the data for the as-synthesized sample is presented as well for a direct comparison. The post heat treatment under the H_2S atmosphere resulted in a nearly three-fold increase in the diffraction intensity of Fe_2GeS_4 NCs as compared to the as-synthesized NCs, indicating a pronounced enhancement in the crystallinity of Fe_2GeS_4 NCs upon annealing. It is important to note that all of the XRD reflections of the post-annealed sample, including very weak ones such as the (211) and (321) peaks, were unambiguously deconvoluted and assigned to the olivine Fe_2GeS_4 phase, as denoted in Fig. 3a. Moreover, the sample heat-treated at 450 °C did not exhibit any trace of a secondary phase, thus alleviating concern over phase decomposition, as is theoretically predicted.[13] The post-annealing process also induced the narrowing of the XRD peaks. According to Scherrer's analysis, the primary particles were estimated to be (23 ± 2) nm and (56 ± 5) nm for the as-synthesized and post-annealed NCs, respectively. The Raman spectra (Fig. 3b) of the as-synthesized Fe_2GeS_4 NCs exhibited only one characteristic scattering at around 361 cm^{-1}, which can be tentatively assigned to the olivine Fe_2GeS_4 phase. As in the XRD patterns, post-annealing resulted in a significant increase in the intensity of this main peak. The tiny satellite peak that appeared at around 345 cm^{-1} after the heat treatment is yet to be indexed, which may indicate possible impurity phases in a minor amount.

Fig. 4 shows TEM images revealing the detailed morphological and crystallographical features of the as-synthesized (a–d) and heat-treated Fe_2GeS_4 NCs (e–h). It is shown that the NCs grew larger after the heat treatment. The as-

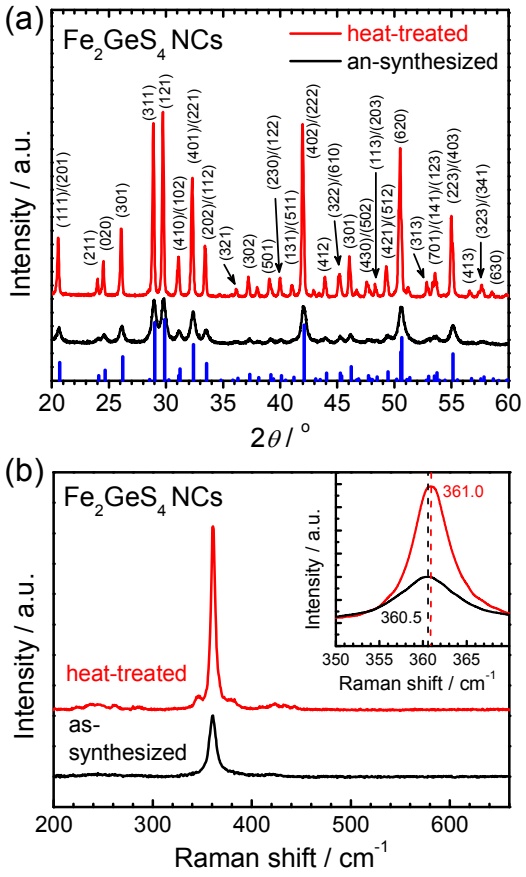

Fig. 3. Comparison of the XRD patterns (a) and Raman spectra (b) of the as-synthesized Fe_2GeS_4 NCs and those post-annealed at 450 °C for 2 h. Note that the vertical bars in part a denote the reference data quoted from JCPDS card no. 04-007-5444 for Fe_2GeS_4.

synthesized NCs ranged in size from 30 to 100 nm, whereas the post-heat-treated NCs ranged from 60 to 200 nm (also see Fig. S3 in the ESI). In addition, the shape of the NCs changed after the heat treatment. The synthesized NCs appear to have a plate-like shape (Figs. 4a and 4b), as previously reported by Fredrick and Prieto.[16] The platelet NCs were observed to become more angular in shape after the post-annealing process (Figs. 4e, 4f, and S4). Some of the heat-treated NCs have a well-defined hexagonal structure, as shown in Fig. 4f. There have been several reports of other chalcogenide NCs having a hexagonal-faceted platelet structure.[24,25] The high-resolution TEM image in Fig. 4c demonstrates that the Fe_2GeS_4 NCs are single-crystalline in nature, clearly showing the lattice fringes. From Fig. 4c and the corresponding reciprocal image (Fig. 4d, obtained by fast Fourier transform, FFT), the interplanar spacings of the lattice fringes were estimated to be 0.26, 0.26, and 0.45 nm, which agree well with the (112), (202), and (011) planes of the olivine Fe_2GeS_4. The *d*-spacings of the post-annealed sample were also in good agreement with the Fe_2GeS_4 phase, as depicted in Figs. 4g and h. However, the post-annealing process gave rise to significant changes in the crystallographic features of the Fe_2GeS_4 NCs. The lattice-resolved image and the SAED pattern (Figs. 4g and 4h) revealed that the six faces of the hexagonal platelet were

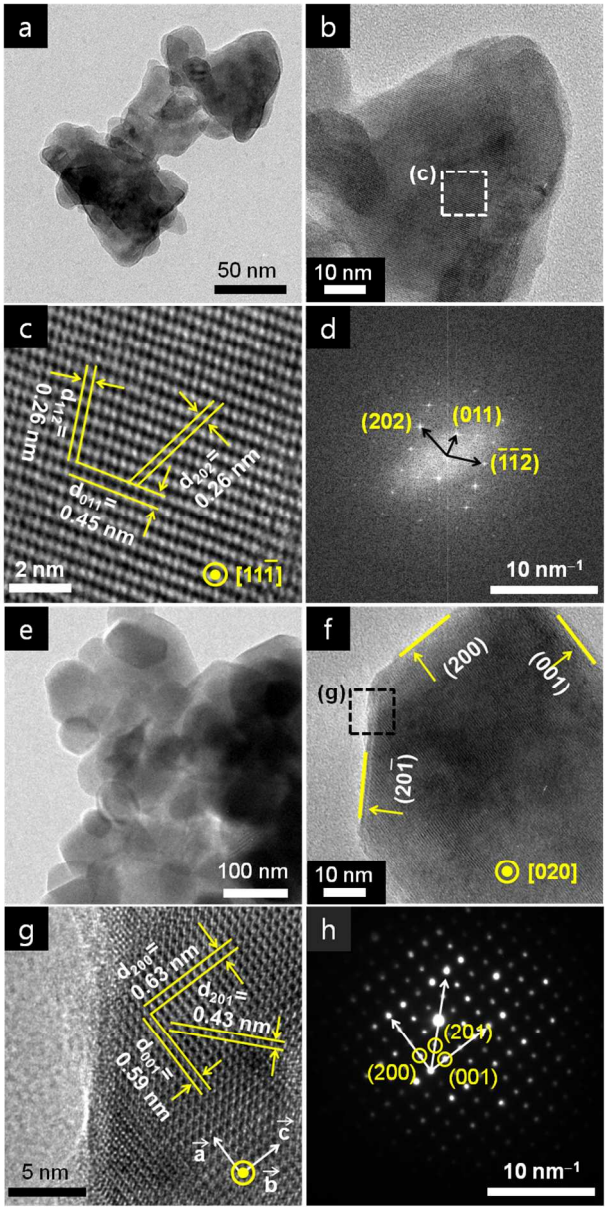

Fig. 4. TEM investigations of as-synthesized (a–d) and heat-treated (e–h) Fe_2GeS_4 NCs. TEM images under low (a and e) and high (b and f) magnification levels, HRTEM images (c and g), and corresponding the fast Fourier transformation image (d) or the selected-area electron diffraction pattern (h).

developed perpendicular to the crystallographic directions of <200>, <001>, and <20-1> with a zone axis along the [020] direction. One may recognize in Fig. 1a that each of the (020) and (040) planes of the Fe_2GeS_4 unit cell contains four sulfur anions (with two iron ions), although the alignment of the atoms on the (020) planes is slightly distorted. Due to the much larger ionic radius of S (1.84 Å) compared to those of Fe (0.78 Å) and Ge (0.39 Å),[26] the (002) or (004) planes have the highest planar density. Thus, it is likely that the crystallographic planes perpendicular to the b-axis are energetically most stable and will tend to be exposed as long as enough kinetic energy is imparted to the constituent atoms. Accordingly, we suggest that the enhanced migration of atoms during the post heat treatment with

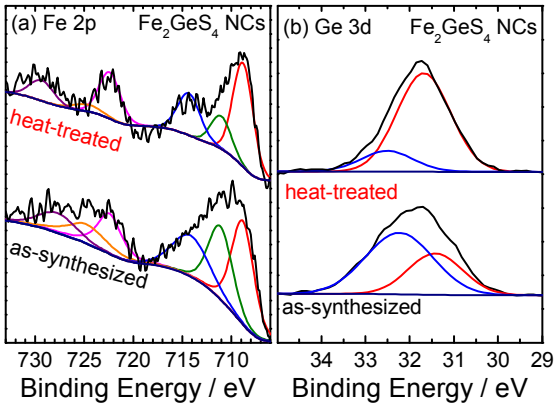

Fig. 5. High-resolution XPS spectra of (a) Fe 2p and (b) Ge 3d from as-synthesized (bottom) and post-heat-treated (top) Fe_2GeS_4 NCs.

a supply of sulfur atoms induced a rearrangement of the atoms towards the most stable structure, thus resulting in faceting and enhanced crystallinity. The enhanced crystallinity observed in the XRD patterns is also supported by the fact that the diffusive bright rings in the SAED pattern disappeared after the heat treatment (Fig. S3).

The present mechanochemical process was not carried out under a controlled oxygen-free atmosphere. Therefore, the Fe_2GeS_4 NCs were likely oxidized to form an oxide layer at the surface, although no oxide phase was identified in the XRD patterns. In order to examine the existence of the oxide layer, the XPS spectra of the Fe_2GeS_4 NCs were measured, as shown in Fig. 5. The Fe 2p spectrum of the as-synthesized NCs revealed the presence of various iron species (Fig. 5a). The intense red- and magenta-colored peaks, located at 709 and 722.5 eV, were assigned to $2p_{3/2}$ Fe(II) sulfide and $2p_{1/2}$ Fe(II) sulfide, respectively, due to the spin-orbit splitting of 13.5 eV.[27] In comparison with these peaks, the peaks with a higher binding energy located at 711.5 (green-colored line) and 725 eV (orange-colored line) can be assigned to oxide-related Fe(II) ions, respectively.[28,29] It was noted that the intensities of these peaks for Fe–O bonds in the as-synthesized NCs were considerably reduced by the post heat treatment. Fig. 5b shows that the Ge 3d peak with a higher binding energy of approximately 32.5 eV, which is associated with Ge–O bonds,[16] also decreased substantially after the post-annealing process. These spectral changes of the XPS data suggest that the post heat treatment induced the formation of sulfide by removing oxygen-related bonds. Comparing our results to the XPS data in a previous report,[16] the as-synthesized NCs in this study had a similar degree of oxidation to those wet-chemically synthesized after air exposure for 12 to 24 h. It appears that the Fe_2GeS_4 NCs are reactive to the point that surface oxidation is inevitable. Fig. 5 shows, however, that they can be easily recovered by the heat treatment proposed in this work.

The enhanced crystallinity and removal of oxygen bonds by the heat treatment resulted in a change in the optical property. Figs. 6a and 6b show k/s versus photon energy ($h\nu$) plots of the as-synthesized and heat-treated NCs as calculated from the reflectance spectra, where k and s denote the absorption coefficient and scattering coefficient, respectively.[30] From Fig. 6b,

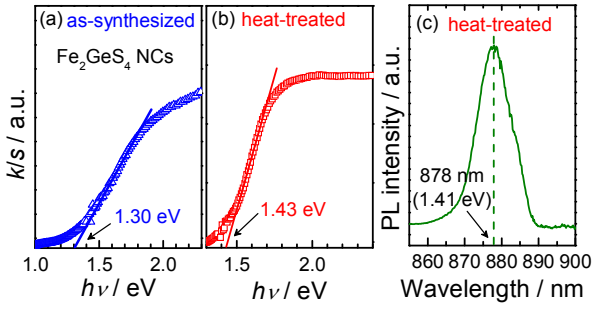

Fig. 6. Diffuse reflectance spectra converted to *k*/*s* of (a) as-synthesized and (b) heat-treated Fe_2GeS_4 NCs. (c) PL spectrum of heat-treated Fe_2GeS_4 NCs.

the band-gap energy of the post-annealed Fe_2GeS_4 NCs was determined to be 1.43 eV, which is in good agreement with the calculated band gap of Fe_2GeS_4, 1.40 eV.[13] The PL spectrum of the heat-treated Fe_2GeS_4 NCs (Fig. 6c) showed an intense near-band-edge emission at 1.41 eV, which is consistent with the above reflectance measurement. In comparison, the band-gap energy of the as-synthesized Fe_2GeS_4 NCs was slightly lower (1.30 eV from Fig. 6a). This can be attributed to the surface oxide layer with a lower band gap and/or the partially amorphous nature of as-synthesized Fe_2GeS_4 NCs.

Conclusions

In summary, we demonstrated the facile synthesis of highly crystalline Fe_2GeS_4 NCs via a solvent-free mechanochemical process. By eliminating tedious processes involving a solution, the present method offers a more rapid and simple route in comparison with solution-based methods. From the time evolution of the crystalline phase and morphology, we found that the formation of Fe_2GeS_4 NCs appears to follow the mechanism of the self-ignition and propagation of chemical reactions. Moreover, we proposed a means of enhancing the crystallinity of the as-synthesized nanoparticles: a post heat treatment in a H_2S atmosphere. It is suggested that the kinetic energy during the heat treatment induced a rearrangement of the constituent atoms towards the most stable configuration, thus resulting in faceting and enhanced crystallinity of the NCs. In addition, the heat treatment was found to eliminate the surface oxide layers. As a result, the post-annealed Fe_2GeS_4 NCs showed a clear absorption edge at 1.43 eV as well as a strong PL signal at 1.41 eV. The observed band-gap energies are near the optimal value in the light of the solar-spectrum utilization, thus offering a promising perspective on Fe_2GeS_4 as a light-absorbing material.

Acknowledgments

This work was financially supported by KIST institutional funding (Project No. 2E24571, 2E24572, 2E24821), by the Korea Research Council of Fundamental Science, Technology (KRCF) for the "National Agenda Project" program, by the KUUC program, and the National Research Foundation of Korea (NRF) grant funded by the Korea government (MSIP) (No. 2007-0056091).

Notes and references

[a] *Center for Materials Architecturing, Korea Institute of Science and Technology, Seoul 136-791, Korea. Fax: +82-2-958-5529; Tel: +82-2-958-5381; E-mail: patra@kist.re.kr*
[b] *Department of Materials Science and Engineering, Korea University, Seoul 136-701, Korea*
[c] *Department of Materials Science and Engineering, Yonsei University, Seoul 120-749, Korea*
[d] *Photo-electronic Hybrids Research Center, Korea Institute of Science and Technology, Seoul 136-791, Korea. Fax: +82-2-958-6649; Tel: +82-2-958-6710; E-mail: dklee@kist.re.kr*
[e] *Department of Nanomaterials Science and Engineering, Korea University of Science and Technology, Daejeon 305-350, Korea*
† Electronic Supplementary Information (ESI) available: SEM images of the powders as a function of the milling time, EDS analysis of as-synthesized nanoparticles, and TEM images and SAED patterns of as-synthesized and heat-treated Fe_2GeS_4 NCs. See DOI: 10.1039/b000000x/
‡ These authors equally contributed to this work.

1 A. Chirila, P. Reinhard, F. Pianezzi, P. Bloesch, A. R. Uhl, C. Fella, L. Kranz, D. Keller, C. Gretener, H. Hagendorfer, D. Jaeger, R. Erni, S. Nishiwaki, S. Buecheler and A. N. Tiwari, *Nat. Mater.*, 2013, **12**, 1107–1111.
2 K. L. Chopra, P. D. Paulson and V. Dutta, *Prog. Photovoltaics*, 2004, **12**, 69–92.
3 M. G. Panthani, J. M. Kurley, R. W. Crisp, T. C. Dietz, T. Ezzyat, J. M. Luther and D. V. Talapin, *Nano Lett.*, 2014, **14**, 670–675.
4 W. Wang, M. T. Winkler, O. Gunawan, T. Gokmen, T. K. Todorov, Y. Zhu and D. B. Mitzi, *Adv. Energy Mater.*, 2014, **4**, 1301465-1−1301465-5.
5 A. Ennaoui, S. Fiechter, C. Pettenkofer, N. Alonsovante, K. Buker, M. Bronold, C. Hopfner and H. Tributsch, *Sol. Energy Mater. Sol. Cells*, 1993, **29**, 289–370.
6 N. Berry, M. Cheng, C. L. Perkins, M. Limpinsel, J. C. Hemminger and M. Law, *Adv. Energy Mater.*, 2012, **2**, 1124–1135.
7 J. Puthussery, S. Seefeld, N. Berry, M. Gibbs and M. Law, *J. Am. Chem. Soc.*, 2011, **133**, 716–719.
8 K. Ramasamy, M. A. Malik, N. Revaprasadu and P. O'Brien, Chemistry of Materials, 2013, **25**, 3551–3569.
9 A. S. Barnard and S. P. Russo, *J. Phys. Chem. C*, 2007, **111**, 11742–11746.
10 M. Birkholz, S. Fiechter, A. Hartmann and H. Tributsch, *Phys. Rev. B: Condens. Matter Mater. Phys.*, 1991, **43**, 11926–11936.
11 C. Steinhagen, T. B. Harvey, C. J. Stolle, J. Harris and B. A. Korgel, *J. Phys. Chem. Lett.*, 2012, **3**, 2352–2356.
12 D. Y. Wang, Y. T. Jiang, C. C. Lin, S. S. Li, Y. T. Wang, C. C. Chen and C. W. Chen, *Adv. Mater.*, 2012, **24**, 3415–3420.
13 L. P. Yu, S. Lany, R. Kykyneshi, V. Jieratum, R. Ravichandran, B. Pelatt, E. Altschul, H. A. S. Platt, J. F. Wager, D. A. Keszler and A. Zunger, *Adv. Energy Mater.*, 2011, **1**, 748–753.
14 W. Shockley and H. J. Queisser, *J. Appl. Phys.*, 1961, **32**, 510–519.
15 S. E. Habas, H. A. Platt, M. F. van Hest and D. S. Ginley, *Chem. Rev.*, 2010, 110, 6571–6594.
16 S. J. Fredrick and A. L. Prieto, *J. Am. Chem. Soc.*, 2013, **135**, 18256–18259.
17 T. Friscic, I. Halasz, P. J. Beldon, A. M. Belenguer, F. Adams, S. A. Kimber, V. Honkimaki and R. E. Dinnebier, *Nat. Chem.*, 2013, **5**, 66–73.
18 V. Sepelak, A. Duvel, M. Wilkening, K. D. Becker and P. Heitjans, *Chem. Soc. Rev.*, 2013, **42**, 7507–7520.
19 K. Ralphs, C. Hardacre and S. L. James, *Chem. Soc. Rev.*, 2013, **42**, 7701–7718.
20 L. Takacs, *Prog. Mater. Sci.*, 2002, 47, 355–414.
21 T. Wada and H. Kinoshita, *J. Phys. Chem. Solids*, 2005, **66**, 1987–1989.
22 X. Ma, W. Yuan, S. E. Bell and S. L. James, *Chem. Commun.*, 2014, **50**, 1585–1587.
23 B. I. Park, Y. Hwang, S. Y. Lee, J. S. Lee, J. K. Park, J. Jeong, J. Y. Kim, B. Kim, S. H. Cho and D. K. Lee, *Nanoscale*, 2014, **6**, 11703–11711.

24 Y. Wu, C. Wadia, W. Ma, B. Sadtler and A. P. Alivisatos, *Nano Lett.*, 2008, **8**, 2551–2555.
25 H. Lee, W. Lee, J. Y. Kim, M. J. Ko, K. Kim, K. Seo, D. K. Lee and H. Kim, *Electrochim. Acta*, 2013, **87**, 450–456.
26 R. D. Shannon, *Acta Crystallogr.*, 1976, **32**, 751–767.
27 S. Seefeld, M. Limpinsel, Y. Liu, N. Farhi, A. Weber, Y. Zhang, N. Berry, Y. J. Kwon, C. L. Perkins, J. C. Hemminger, R. Wu and M. Law, *J. Am. Chem. Soc.*, 2013, **135**, 4412–4424.
28 D. Brion, *Appl. Surf. Sci.*, 1980, **5**, 133–152.
29 M. Descostes, F. Mercier, N. Thromat, C. Beaucaire and M. Gautier-Soyer, *Appl. Surf. Sci.*, 2000, **165**, 288–302.
30 J. D. Lindberg and D. G. Snyder, *Appl. Opt.*, 1973, **12**, 573–578.

Table of content entry

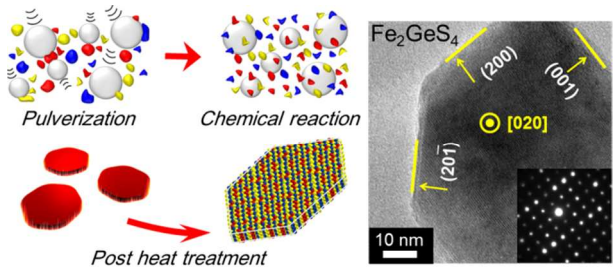

Highly crystalline Fe_2GeS_4 nanocrystals were synthesized via a facile, solvent-free mechanochemical process. The post-annealed Fe_2GeS_4 nanocrystals showed an absorption edge at 1.43 eV and a PL emission at 1.41 eV.